

Available online at website: https://journal.bcrec.id/index.php/bcrec

Bulletin of Chemical Reaction Engineering & Catalysis, 20 (1) 2025, 177-192



Research Article

Visible-light Degradation of Methylene Blue using Energy-Efficient Carbon-Doped TiO₂: Kinetic Study and Mechanism

Alysa Lau¹, Chien Yong Goh², Yubei Guo¹, Abdulkareem Ghassan Alsultan³, Yun Hin Taufiq-Yap³, Mukhamad Nurhadi⁴, Sin Yuan Lai^{1,5,*}

¹School of Energy and Chemical Engineering, Xiamen University Malaysia, Jalan Sunsuria, Bandar Sunsuria, 43900 Sepang, Selangor, Malaysia.

²Department of Mathematics, Xiamen University Malaysia, Jalan Sunsuria, Bandar Sunsuria, 43900 Sepang, Selangor, Malaysia.

³Catalysis Science and Technology Research Centre (PutraCat), Faculty of Science, Universiti Putra Malaysia, 43400 Serdang, Selangor Darul Ehsan, Malaysia.

⁴Department of Chemical Education, Universitas Mulawarman, Kampus Gunung Kelua, Samarinda, 75119, East Kalimantan, Indonesia.

⁵College of Chemistry and Chemical Engineering, Xiamen University, 361005 Xiamen, China.

Received: 1st February 2025; Revised: 3rd March 2025; Accepted: 4th March 2025 Available online: 6th March 2025; Published regularly: April 2025



Abstract

Wastewater pollution is mainly produced from the dye textile industry and the most widely used photocatalyst to degrade dye textile is TiO₂ due to its photostability, low toxicity, and low production cost. However, TiO₂ is only responsive under UV light; thus, our study is to extend the TiO₂ absorption light to visible region via doping of biobased carbon source, viz. ascorbic acid, to produce carbon-doped TiO₂. The carbon-doped TiO₂ were solvothermally synthesized with varying carbon loadings (10, 30, and 50 wt%) and calcination temperatures (250, 300, and 400 °C). The functional groups of carbon-doped TiO₂ were determined, which the carbonyl groups (C=O) at 1700 cm⁻¹, alkenyl groups (C=C) at 1630-1670 cm⁻¹, hydroxyl groups at 3380-3390 cm⁻¹, and TiO₂ appeared at 450 cm⁻¹. The absorption spectra shifted from UV to visible-light region and the band gap was reduced compared to undoped TiO₂. The photoluminescence results showed that the surface oxygen vacancies (SOVs) are generated for carbon-doped TiO₂. The Ti–C bond formation was proved through diffractogram peak shifting, while the crystallite sizes decrease with increasing carbon amount and decreasing calcination temperature. The highest methylene blue photodegradation of 89.53% was achieved by 30 wt%C-TiO₂-250 photocatalyst at pH 10 under 2 h visible light irradiation.

Copyright © 2025 by Authors, Published by BCREC Publishing Group. This is an open access article under the CC BY-SA License (https://creativecommons.org/licenses/by-sa/4.0).

Keywords: Carbon-doped TiO₂; green synthesis; dye photodegradation; wastewater; band gap; environmental sustainability

How to Cite: Lau, A., Goh, C. Y., Guo, Y., Alsultan, A. G., Yun Hin, T., Nurhadi, M., Lai, S. Y. (2025). Visible-light Degradation of Methylene Blue using Energy-Efficient Carbon-Doped TiO₂: Kinetic Study and Mechanism. Bulletin of Chemical Reaction Engineering & Catalysis, 20 (1), 177-192. (doi: 10.9767/bcrec.20347)

Permalink/DOI: https://doi.org/10.9767/bcrec.20347

1. Introduction

In the 21st century, the major global concern is to provide and ensure the cleanliness of water supply for the whole ecosystem. Water contamination is mainly caused by the expansion

of industrialization. Among all of the industries, textile dyeing is the second-largest polluter of water worldwide, with the fashion industry producing 20% of the world's wastewater alone [1,2]. The issue is currently encountered by the countries relying on textile dyeing industry, such as China, Bangladesh, Thailand, and Indonesia. The textile manufacturers use large amounts of water and the resulting wastewater produces

^{*} Corresponding Author. Email: sinyuan.lai@xmu.edu.my (S.Y. Lai)

highly polluted discharge [1]. Most dye effluents are highly poisonous and non-biodegradable, and thus giving rise to significant negative impacts on the environment, aquatic and human life.

Photocatalysis, a green chemistry technology, has drawn a lot of attention due to its emerging materials in potentially wastewater treatment, including textile dye effluents. The photocatalytic concept is about semiconductors to absorb sufficient photon energy and create electron-hole pairs, whereby the excited electrons jump from valence band to conduction band to overcome the band gap edges. The photocatalysis involves redox reaction, which the electrons act as the reducing agents while the positive holes act as the oxidizing sites. The water and oxygen molecules or oxygencarrier reagents adsorb on the catalyst surface to generate hydroxyl radicals (HO·) and reactive oxygen radicals (ROS) [3]. The dye pollutants that adsorb onto the catalyst surface are decomposed by the HO· and ROS to generate less hazardous chemicals or mineralize to non-hazardous CO2 and water.

semiconductors Among used photocatalysis, TiO2 is the most promising semiconductor in photocatalytic dye degradation due to its high chemical stability, high oxidizing power, low cost, and environmental friendliness [3–5]. Compared to other wastewater treatment methods, such as ozonolysis, which requires a high-power supply and leads to intensive coal combustion, or biological treatment, which generates irritating biogases, TiO2 photocatalysis presents a more sustainable alternative. This approach utilizes solar energy as its primary power source, making it an environmentally friendly and energy-efficient solution. Nonetheless, TiO₂ semiconductor poses key drawbacks, i.e. wide band gap and fast electronhole recombination rate, that restraining its wide applications. It can only absorb 5% UV light of the solar spectrum owing to wide band gap (3.2 eV), while the fast electron-hole recombination causes low HO· and ROS generation for degradation. Lots of endeavors have been devoted to narrow the band gap and reduce charge recombination, such as metal doping [6–8], non-metal doping [9–11], dye-sensitizing [12,13], etc.

The metal doped TiO₂ could reduce the electron-hole recombination rate but increasing charge trapping in TiO₂ [5] and lower thermal stability [4]. Besides, the dye-sensitized TiO₂ is not appropriately used for dye degradation [4], might due its low durability and reusability upon prolonged exposure to chemicals, temperature and light, this will subsequently affect the effective of TiO₂ in photocatalytic activity. Intriguingly, the non-metal dopants exhibit higher thermal stability and no charge trapping issue (better charge transfer) [5]. One of the non-metal doping is using carbon sources, such as

ethanol [4,5,14], glucose [15–17], propanol [18], starch [19] and glycol [20], have been carried out by researchers to dope or modify the TiO₂ catalyst using reverse microemulsion [21], chemical vapor deposition [22], carbonization [16], sol-gel [3,5], and hydrothermal/solvothermal [4,23–25]. Among these methods, hydrothermal / solvothermal treatments offer greater control over the synthesis process, resulting in a more homogeneous structure with strong chemical bonding. Additionally, these methods are advantageous due to their simplicity, relatively short reaction times, and operation within an acceptable temperature range, making them efficient and practical for material synthesis. It is reported that the carbon atoms substitute the oxygen lattice in TiO₂ to give oxygen vacancies and Ti-C bonds, causing charges are trapped and transferred for a better photocatalytic efficiency [3].

In detail, the surface modification that has been investigated mostly are carbohydrates and alcohols with hydroxyl groups (-OH), which are common carbon sources for TiO2 doping. The hydroxyl group (-OH) in carbohydrates and alcohols can form oxidative hydroxyl radicals (•OH) as the principal oxidants in photodegradation, enhance thus the photocatalytic performance [26]. Additionally, carbon doping can narrow the band gap for expanding to visible light activation, and withdraw electron to increase electron flow for higher immobilization [19]. For instances, glucose and starch as the carbohydrate carbon source to significantly improve the photocatalytic activity [27,28] and the removal of anionic Orange II was improved by the butanol-modified TiO₂ applying alcohol as the carbon source [29].

As the efficiency of carbon source with solely hydroxyl group still can be improved, this research tends to study carboxylic acid compounds with carboxyl groups (-COOH), which comprised of both hydroxyl and carbonyl group (C=O), to produce a visible light-responsive TiO₂. Among them, ascorbic acid is chosen to modify TiO2 lattice as the natural availability and simple technology. The bidentate carboxylate ligand O-Ti-C is a strong electron-withdrawing group contributing to better charge separation and interfacial charge transfer efficiency; hence the photocatalytic performance could be improved. Ascorbic acid has only been employed once as carbon-doping TiO₂ via incipient wet impregnation and achieved ideal hydroquinone photocatalytic degradation rate

To the best of our knowledge, no research reports on using ascorbic acid as TiO₂ carbon dopant through solvothermal-calcination approach. Hence, our research demonstrates the structural modification of TiO₂ lattice with ascorbic acid, aiming to produce a carbon-doped

TiO₂ with narrower band gap, reduced electronhole recombination rate, and enhanced interfacial charge transfer. The different loadings of carbondoped TiO₂ using ascorbic acid are studied through solvothermal process under different calcination temperatures. Then, a series of characterizations to investigate the physicochemical properties, such as band gap, crystalline phases, functional group and charge transfer, are followed. Lastly, the photocatalytic activity of carbon-doped TiO₂ is evaluated by the degradation with methylene blue (MB) under 300 W visible light irradiation for 2 h.

This study serves as a foundation for the broader development of photocatalytic technology by addressing key aspects such as material optimization, mechanistic insights, and the Adegradation of diverse pollutants. Firstly, the doping of TiO2 can modify its surface and intrinsic properties, enabling it to absorb light at longer wavelengths with lower energy requirements, thereby enhancing its photocatalytic efficiency. Secondly, investigating reaction pathways and photodegradation kinetics provides valuable insights into process optimization, facilitating the application of photocatalysis across various fields. Lastly, the applicability of photocatalysis extends beyond dye degradation to a wide range of pollutants, including pesticides, pharmaceuticals, and heavy metals, demonstrating its versatility as advanced environmental remediation technology.

2. Materials and Method

2.1 Materials

Acetic acid (100%, glacial, Sigma-Aldrich), ethanol (95%, Sigma-Aldrich), absolute ethanol (Sigma-Aldrich), titanium (IV) butoxide (98%, Sigma-Aldrich), and ascorbic acid (Sigma-Aldrich).

2.2 Method

2.2.1 Catalyst preparation

1 mL of acetic acid was added into 10 mL distilled water and 6 mL of titaniu(IV) butoxide, $Ti(C_4H_9O)_4$ (MW = 340.32 g.mol⁻¹) was added into 20 mL of 95% ethanol. After that, acetic acid solution was added dropwise into the TiO2 solution to acid-catalyze the formation of titanium sols through hydrolysis. The titanium sols were then sonicated for 10 min and stirred vigorously for 20 min to promote the condensation reaction (Figure 1). While waiting for the TiO₂ formation, the ascorbic acid (10 wt%, MW = 176.124 g.mol⁻¹) was dissolved in 20 mL absolute ethanol. The assynthesized TiO2 solution was then mixed with ascorbic acid (10 wt%). The mixture solution was transferred to a 100 mL Teflon-lined stainlesssteel autoclave. The autoclave was put inside the oven for solvothermal treatment at 160 °C for 10 h. After 10 h, the Teflon-lined stainless-steel autoclave was allowed to cool to room temperature. The as-synthesized precipitate was

Reaction 1: Hydrolysis of titanium (IV) butoxide

$$C_4H_9O$$
 — Ti — OC_4H_9 + $4H_2O$ — OC_4H_9 + $4C_4H_9OH$ — OC_4H_9 — OC_4H_9

Reaction 2: Condensation of titanium (IV) butoxide

Overall reaction

$$C_4H_9O$$
 Ti
 OC_4H_9
 CH_3COOH
 $TiO_2 + 4 C_4H_9OH$
 OC_4H_9

Figure 1. Hydrolysis and condensation reaction of titanium(IV) butoxide to form TiO₂.

collected by centrifuging repeatedly and washed with ethanol and distilled water for three times. The fine powder was obtained after drying the collected precipitate in an oven for overnight. The dried, fine powder (carbon-doped TiO₂) was calcined in a muffle furnace at 250 °C.

The same steps above were repeated for ascorbic acid with 30 and 50 wt% and calcination temperatures at 300 and 400 °C. The denotation is as such, x wt%C-TiO_{2-y} with x = loading amount and y = calcined temperature, as shown in Table 1.

2.2.2 Characterizations

The photocatalysts were characterized by double beam Diffuse Reflectance-Ultraviolet Visible (DR-UV VIS, brand: Shimadzu) with the range of 200 nm to 800 nm. BaSO4 is used as the reference to determine the baseline. Ensure that the powder is evenly dispersed to fully cover the mirror of the sample holder. The DR-UV Vis spectrophotometer was setup with 200 nm/min of scanning speed. A wavelength (x-axis) vs absorbance (y-axis) curve is plotted and Tauc Plot is plotted out using these equations, $E=1240/\lambda$ on the x-axis and (ahu)2 on the y-axis. The n=1/2 is used due to its direct allowed transition. Extrapolation is carried out in the linear region of the plot to the x-axis and the point at which it intersected was determined. The band gap values are then determined from the Tauc plot.

The Spectrum One Fourier Transform Infrared Spectroscopy (FTIR, brand: Perkin Elmer) with KBr pellets was used to characterize all of the photocatalyst samples within the range of 400 to 4000 cm⁻¹. The scanning rate was set as 4 cm⁻¹. A mixture of 1:100 catalyst to KBr was prepared and finely crushed into a fine powder under clean conditions. Subsequently, the catalyst/KBr blend was pressed into a thin pallet under 10 ton of pressure using a hydraulic press. The pellet was then loaded into the sample compartment of the FTIR instrument for analysis.

Table 1. The denotations of carbon-doped TiO₂

Catalyst denotation	Ascorbic acid (wt%)	Calcination temperature (°C)
$10 wt\% C\text{-TiO}_2\text{-}250$	10	250
$30wt\%C\text{-TiO}_2\text{-}250$	30	250
$50wt\%C\text{-}TiO_2\text{-}250$	50	250
$10wt\%C\text{-TiO}_2\text{-}300$	10	300
$30wt\%C\text{-TiO}_2\text{-}300$	30	300
$50 \text{wt}\%\text{C-TiO}_2\text{-}300$	50	300
$10wt\%C-TiO_2-400$	10	400
$30wt\%C\text{-TiO}_2\text{-}400$	30	400
$50 \text{wt}\%\text{C-TiO}_2\text{-}400$	50	400

XRD patterns of samples were evaluated using a Bruker analyzer (D8 Advance). The carbon-doped TiO_2 photocatalysts were analyzed with a spectrum range of $20{-}80^{\circ}$ using DIFFRAC.EVA diffractometer having Cu-Ka radiation (I = 30 mA, V = 40 kV). The Debye-Scherrer equation (Equation (1)) was used to calculate the crystallite size of the as-synthesized carbon-doped TiO_2 .

$$D = \frac{k\lambda}{\beta\cos\theta} \tag{1}$$

where, D is the crystallite size of plane (101) for anatase TiO₂, K is the Scherrer constant, 0.94, for spherical crystallite, λ is the X-ray wavelength, Cu-K α = 1.5406 Å (0.15406 nm), β is the full width at half-maximum height (FWHM) of the peak in radians, and θ is the Bragg's angle in degrees, half of 2 θ .

Photoluminescence (PL) emission spectra were measured on a Raman spectrometer at room temperature with the Xenon lamp at the excitation light of 325 nm. The PL spectra in the range of 200-600 nm were investigated.

2.2.3 Photocatalytic activity

25 ppm methylene blue (MB) solution was prepared by weighing 12.5 mg of MB and dissolving in 500 mL of volumetric flask. It was then transferred to a 500 mL photoreactor and the solution was added with 1 M NaOH to obtain pH of 10. 10 mL of 5 mM H₂O₂ and 0.1 g photocatalyst were added into the photoreactor containing 25 ppm of MB. Dark condition was conducted to investigate the adsorption-desorption equilibrium state. 3 mL aliquot was taken out using a syringe filter (0.22 µm pore size) for 10-min intervals until adsorption-desorption equilibrium was reached. UV-vis spectroscopy was used to measure the absorbance. After 30-min of dark condition, 300 W of visible light was switched on. During the photocatalytic process, 3 mL aliquot was taken out every 20-min interval until 2 h. The photocatalytic activity was determined using the equation (C_0 - C_t/C_0) × 100%, where C_0 is the initial MB concentration and C_t is the remaining MB concentration. Figure 2 is an overview on the procedure of carrying out photocatalysts evaluation.

3. Results and Discussions

3.1 Fourier Transform Infrared Spectroscopy (FTIR) Analysis

The FTIR spectra is used to determine the functional groups, such as –OH, C=O, C=C, and C–O, appear on TiO₂ because they are vital for pollutant adsorption and charge transfer enhancement. In Figure 3(a), the cyclic alkene of

C=C band contributed by ascorbic acid is stretching at 1622 cm⁻¹, O-H stretching at 3380 cm⁻¹ due to adsorbed water molecules and hydroxyl groups by ascorbic acid, and O-Ti-O stretching at 450 cm⁻¹ [31]. The 30wt%C-TiO₂-250 has the highest photocatalytic activity of 89.53%, followed by 50wt%C-TiO₂-250 with 86.82%, because of the carbon has interrupted the TiO₂ framework and the presence of carbon-containing functional groups could scavenge the excitons to facilitate charge separation and transmission. In Figure 3(b), it also consists of tetrasubstituted C=C stretching at 1670 cm⁻¹, O-H stretching at

 $3390~cm^{\text{-}1}$ and O–Ti–O stretching at $450~cm^{\text{-}1}$. The $50wt\%\text{C-TiO}_2\text{-}300, 30wt\%\text{C-TiO}_2\text{-}300$ and $10wt\%\text{C-TiO}_2\text{-}300$ show a better photocatalytic activity compared to pure TiO₂, due to the absence of O=C=O at a higher calcination temperature [32] and successful incorporation of carbon into TiO₂ lattice. Figure 3(c) displays the similar absorption peaks, namely C=C stretching at 1670 cm $^{\text{-}1}$, O–H stretching at 3380 cm $^{\text{-}1}$ and O–Ti–O stretching at $450~cm^{\text{-}1}$.

Pure TiO_2 with different calcination temperatures have the same trend in Figure 4(a). It can be observed that all of them consist of C=C

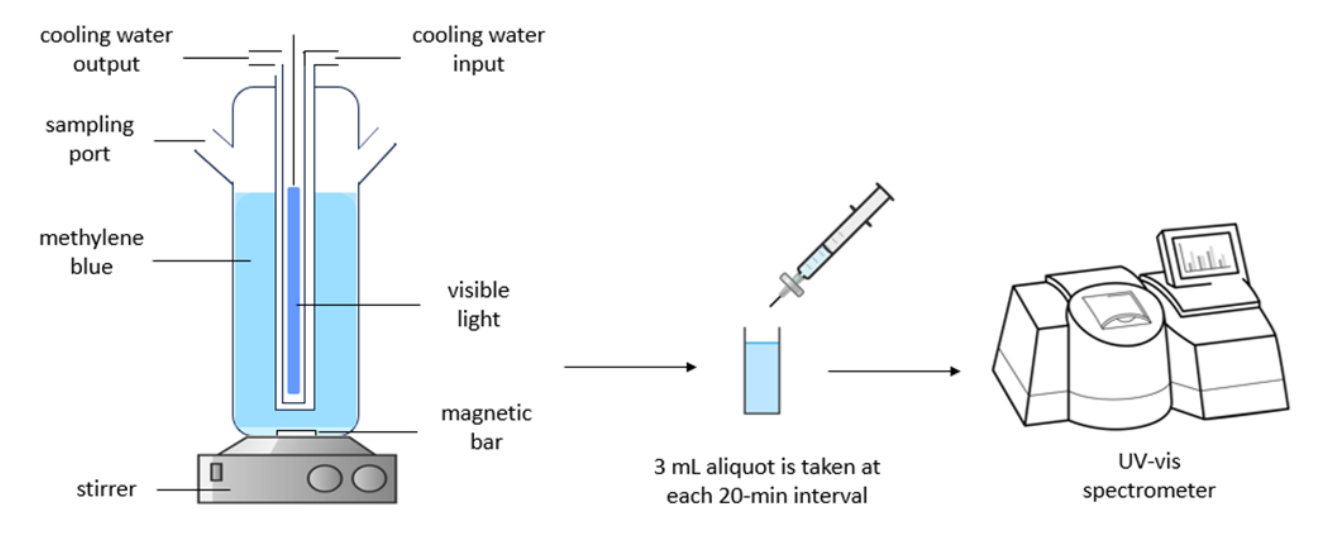


Figure 2. Photodegradation of methylene blue using carbon-doped TiO₂ under visible light irradiation.

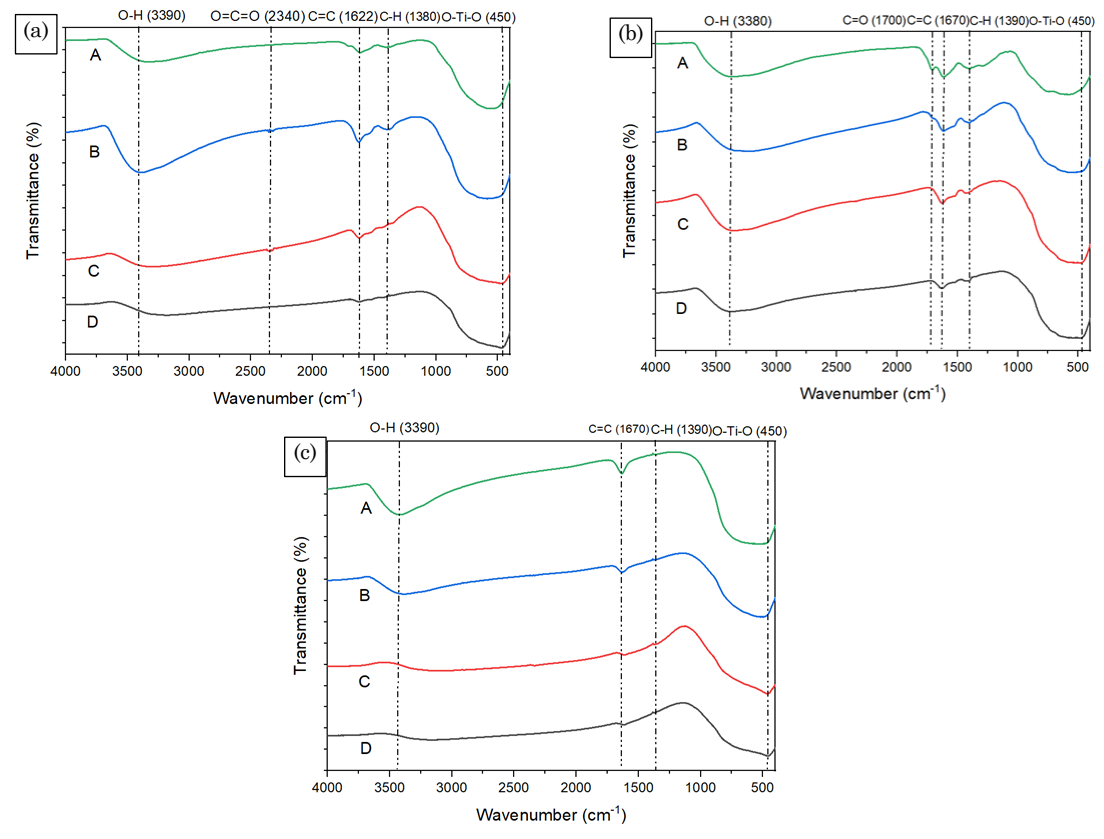


Figure 3. FTIR spectra for TiO_2 with (A) 50 wt%, (B) 30 wt%, (C) 10 wt% of carbon dopants and (D) undoped at (a) 250, (b) 300, (c) 400 °C.

stretching at 1630 cm⁻¹, O-H stretching at 3370 cm⁻¹ and O-Ti-O stretching at 450 cm⁻¹ [31]. In Figure 4(b), TiO₂ with 10 wt% carbon dopants at different calcination temperatures consist of almost the same bond stretching as pure TiO₂, such as C-C stretching at 1640 cm⁻¹, O-H stretching at 3390 cm⁻¹, O-H bending at 1390 cm⁻¹, and O-Ti-O stretching at 450 cm⁻¹. In Figure 4(c), 30wt%C-TiO₂ exhibits the similar absorption bands as Figure 4(b), which consisting of C=C stretching at 1640 cm⁻¹, O-H stretching at 3390 cm⁻¹, O-H bending at 1390 cm⁻¹, and O-Ti-O stretching at 450 cm⁻¹. The photocatalytic activity is the highest at 89.53% contributed by 10wt%C-TiO₂-250 because the presence of C=O and C=C that could trap and transfer electrons to facilitate charge separation. Figure 4(d) shows 50wt%C-TiO₂ at a higher calcination temperature, i.e. 400, has C=C stretching at 1640 cm⁻¹, O-H stretching at 3390 cm⁻¹, C–H stretching at 1380 cm⁻¹, and O– Ti-O stretching at 450 cm⁻¹, but no C=O stretching. At lower calcination temperatures of 250 and 300 °C, the C=O stretching appears at 1700 cm⁻¹, indicating its significant to give a higher photodegradation at 86.82% (50wt%C-84.96% (50wt%C-TiO₂-300), $TiO_2-250)$ and respectively; however, 50wt%C-TiO2-400 gave only 44.11% of MB photodegradation. FTIR spectra demonstrates that carbonyl (C=O) groups play a crucial role in enhancing MB adsorption on C-TiO₂ surfaces through π - π interaction with the

aromatic ring of MB. Moreover, hydroxyl (OH) groups influence electrostatic charges on ${\rm TiO_2}$ surface, inducing it more negatively charges in the alkaline condition and thus, stronger attraction towards MB cationic dye.

3.2 X-ray Diffraction (XRD) Analysis

Figure 5 shows XRD diffractogram of calcination temperatures (250, 300, and 400 °C) on carbon-doped TiO₂ with different loadings amount of ascorbic acid at (a) 10 wt%, (b) 30 wt%, and (c) 50 wt%. All these diffractograms are assigned to anatase TiO2 (JCPDS file no. 21-1272), where the characteristic peaks are observed at 25.3° (101), 37.8° (004), 48.0° (200), 53.8° (105), 55.0° (211), 62.6° (204), 68.6° (116), 70.2° (220), and 75.1° (215). There is only anatase phase observed and no rutile phase of TiO2 could be found in the diffractogram. It is because the rutile phase appears when the calcination temperature reaches more than 400 °C [33], which could cause inferior photocatalytic activity. It is observed that intensity of the peak is higher and width of the peak is narrower with increasing of calcination temperatures at the corresponding carbon loadings of 10, 30 and 50 wt%. This phenomenon is also reported by another research group [32]. To explain this observation, the crystallite sizes are calculated and listed in Table 2. Table 2 displays the crystallite sizes of respective carbon-doped

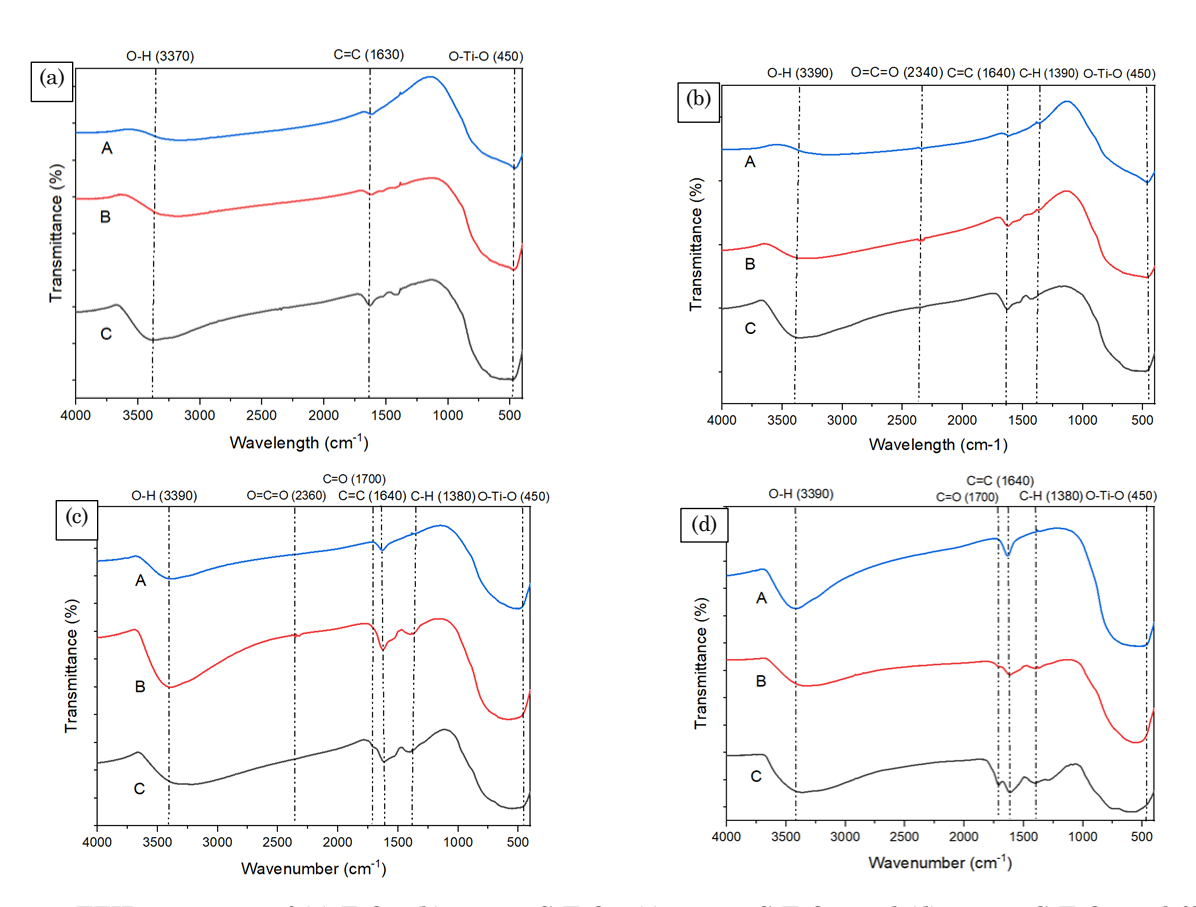


Figure 4. FTIR spectrum of (a) TiO₂, (b) 10wt%C-TiO₂, (c) 30wt%C-TiO₂, and (d) 50wt%C-TiO₂ at different temperatures at (A) 400 °C, (B) 300 °C and (C) 250 °C.

TiO₂ of 10, 30, and 50 wt%, with elevating calcination temperatures of 250, 300 and 400 °C. The increment of the calcination temperature could increase the crystallite sizes of the carbondoped TiO₂, which aligned with the findings from the other literatures [15,33]. The increase of the crystallite size is caused by thermally promoted growth, smaller crystalline possibly the crystalline anatase TiO2 grows after nucleation via Ostwald ripening or combination of smaller primary crystals into larger secondary crystals [32].

Figure 6 shows XRD diffractogram of carbon loadings (10, 30, and 50 wt%) on TiO² at different calcination temperatures of (a) 250 °C, (b) 300 °C,

Table 2. The crystallite sizes of carbon-doped TiO₂ at different calcination temperatures.

Catalyst	Crystallite size (nm)
10wt%C-TiO ₂ -250	4.80
$10 \mathrm{wt}\%\mathrm{C}\text{-TiO}_2\text{-}300$	4.89
$10 \mathrm{wt}\%\mathrm{C}\text{-TiO}_2\text{-}400$	5.03
$30 \mathrm{wt}\%\mathrm{C}\text{-TiO}_2\text{-}250$	3.43
30wt%C-TiO ₂ -300	4.47
$30 \mathrm{wt}\% \mathrm{C}\text{-TiO}_2\text{-}400$	8.94
$50 \mathrm{wt\%C} ext{-TiO}_2 ext{-}250$	2.09
$50 \mathrm{wt\%C}\text{-TiO}_2\text{-}300$	6.59
50wt%C-TiO ₂ -400	4.49

and (c) 400 °C. All these diffractograms are assigned to anatase TiO₂ (JCPDS file no. 21-1272), where the characteristic peaks are observed at 25.5° (101), 38.1° (004), 48.2° (200), 54.4° (105), 55.5° (211), 63.1° (204), 69.3° (116), 70.7° (220) and 75.4° (215). The undoped TiO₂ and carbon-doped TiO₂ gave slightly different degree at the anatase phase (101). Figure 6(a) obviously depicts the peaks are slightly shifted to lower degree with increasing of carbon loadings under the same calcination temperature. This shifting indicates the carbon has been successfully interrupt the TiO₂ lattice to give Ti-C bond. It is reported that the bond length of Ti-C (2.008 and 2.21 Å) is longer than Ti-O (1.942 and 2.002 Å) and the C4radius is also larger than O2- in the TiO2 framework [4]. At a higher temperature of 400 °C, the carbon doping effect to the shifting is less due to the carbon is almost fully decomposed, thus less Ti-C bond could be formed. The similar phenomenon of lower degree shifting is also reported by the research group [4].

Table 3 displays the crystallite sizes of respective carbon-doped TiO₂ at 250, 300 and 400 °C calcination temperatures, with elevating carbon loadings of 10, 30 and 50 wt%. Under the calcination temperature of 250 °C, the increment of carbon loadings could decrease the crystallite sizes owing to the carbon insertion could inhibit the TiO₂ crystal growth, which has been discussed by other studies as well [4,32,33]. However, at

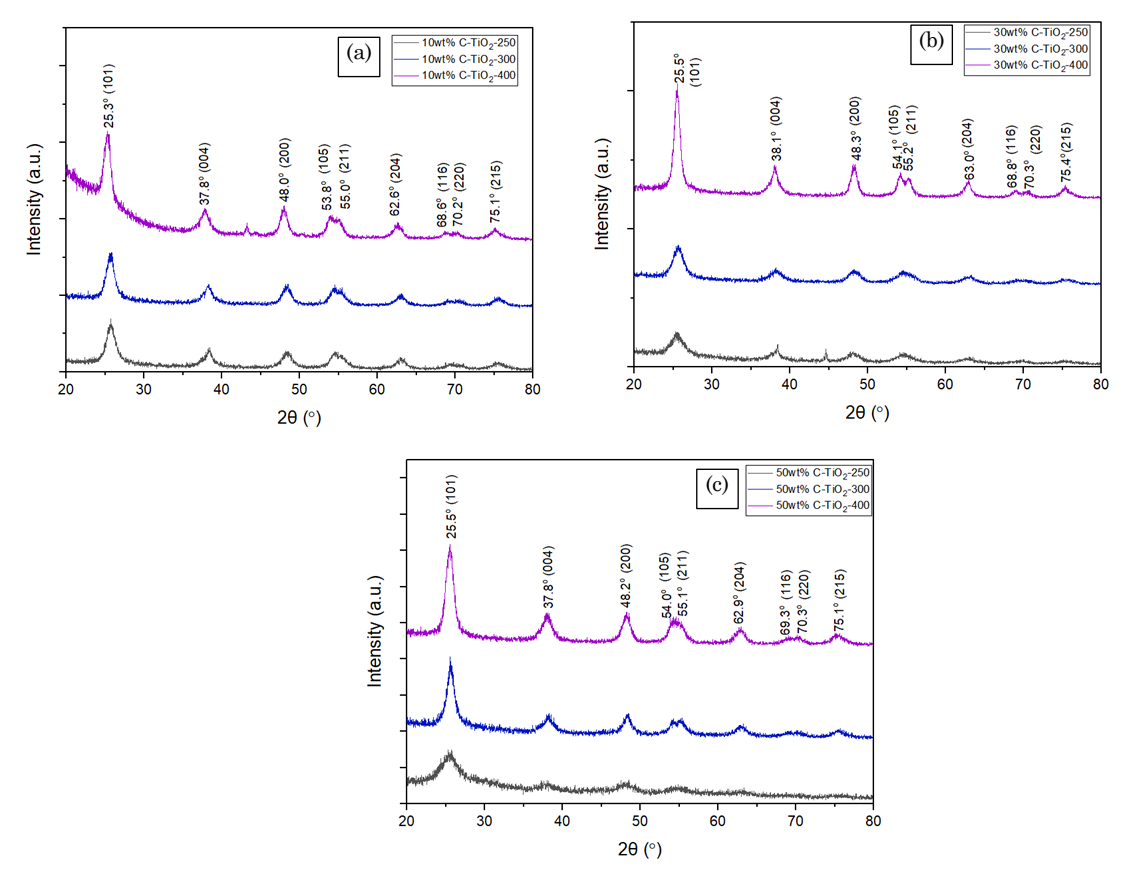


Figure 5. XRD diffractogram of calcination temperatures (250, 300, and 400 °C) on carbon-doped TiO₂ with different loadings amount of ascorbic acid at (a) 10 wt%, (b) 30 wt%, and (c) 50 wt%.

higher calcination temperatures of 300 and 400 °C, the crystallite sizes are not reduced which might be attributed to dissimilar boundaries (grain boundary defects) created by carbon doping [32]. The broader diffractogram with a smaller crystallite size could give a greater number of grain boundary defects [32].

3.3 DRUV-Vis Analysis

Figure 7(a) and Table 4 show the band gaps of carbon-doped TiO₂ calcined at 250 °C are decreasing: 2.80 (undoped TiO₂-250 and 10wt%C-TiO₂-250), 1.88 (30wt%C-TiO₂-250) and 1.73 eV

(50wt%C-TiO₂-250) when the carbon dopants increase from 0 wt% to 50 wt%. The band gaps with 1.88 eV and 1.73 eV showed higher photocatalytic degradation with 89.53% and 86.82%, respectively. A narrower band gap results in higher photocatalytic activity because less energy required for electrons to travel from the valence band to conduction band, which allows more electron-hole pair to be generated [34]. On the contrary, when the band gap is too small, the recombination rate of electron-hole pairs is higher, hence resulting in lower photocatalytic activity. Although TiO₂-250 and 10wt%C-TiO₂-

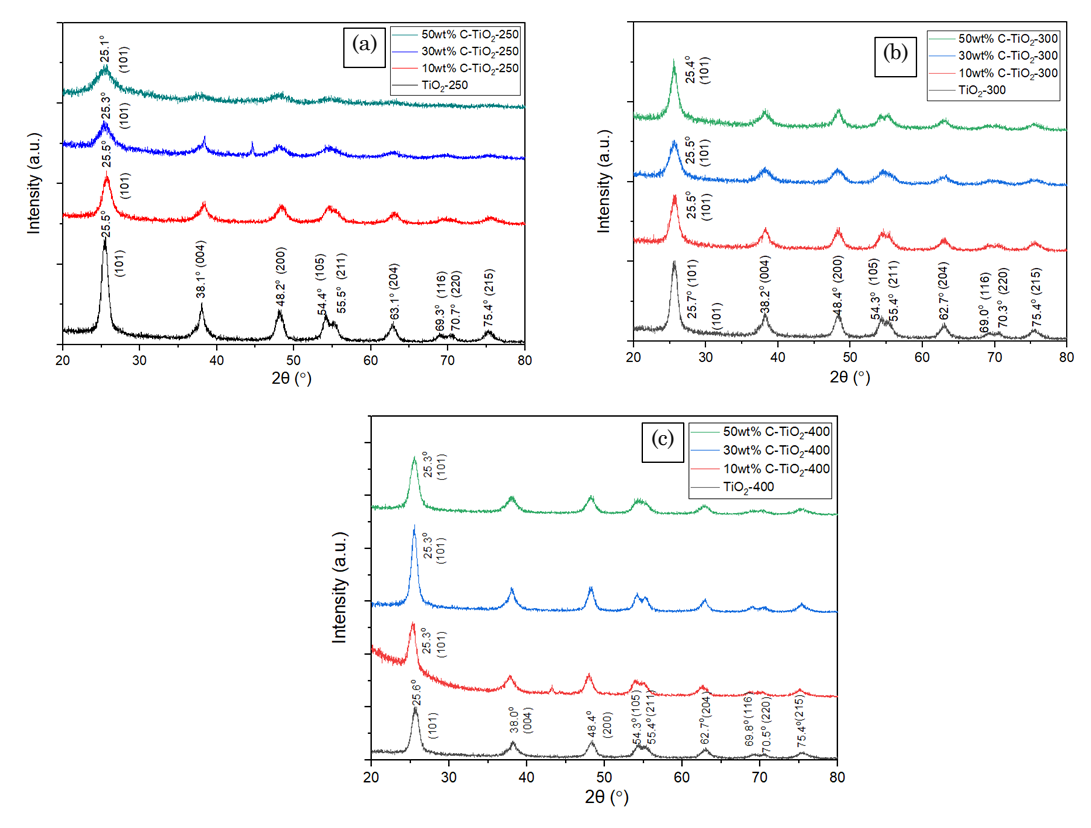


Figure 6. XRD diffractogram of carbon loadings (10, 30, and 50 wt%) on TiO₂ at different calcination temperatures of (a) 250 °C, (b) 300 °C, and (c) 400 °C.

Table 3. The crystallite sizes of undoped TiO₂ and carbon-doped TiO₂ at 10, 30, and 50 wt% with their respective calcination temperatures.

Catalyst denotation	Crystallite size (nm)
TiO ₂	7.54
$10 wt\% C\text{-TiO}_2\text{-}250$	4.80
$30 \mathrm{wt}\%\mathrm{C}\text{-TiO}_2\text{-}250$	3.43
$50\mathrm{wt}\%\mathrm{C} ext{-}\mathrm{TiO}_2 ext{-}250$	2.09
$10 \mathrm{wt}\%\mathrm{C}\text{-TiO}_2\text{-}300$	4.89
$30 \text{wt}\%\text{C-TiO}_2\text{-}300$	4.47
$50 \mathrm{wt}\%\mathrm{C} ext{-}\mathrm{TiO}_2 ext{-}300$	6.59
$10 \mathrm{wt}\%\mathrm{C}\text{-TiO}_2\text{-}400$	5.03
$30 \text{wt}\%\text{C-TiO}_2\text{-}400$	8.94
50wt%C-TiO ₂ -400	4.49

Table 4. Band gaps of undoped TiO_2 and carbondoped TiO_2 .

Photocatalyst	Band Gap (eV)
${ m TiO_2\text{-}250}$	2.80
$10\mathrm{wt}\%\mathrm{C} ext{-}\mathrm{TiO}_2 ext{-}250$	2.80
$30 \mathrm{wt}\%\mathrm{C}\text{-TiO}_2\text{-}250$	1.88
$50 \mathrm{wt\%C\text{-}TiO_2\text{-}}250$	1.73
TiO_2 -300	3.05
10wt%C-TiO ₂ -300	3.00
30wt%C-TiO ₂ -300	2.86
$50 \mathrm{wt}\%\mathrm{C}\text{-TiO}_2\text{-}300$	2.66
${ m TiO_{2}} ext{-}400$	3.00
$10 \mathrm{wt}\%\mathrm{C}\text{-TiO}_2\text{-}400$	3.05
$30 \text{wt}\%\text{C-TiO}_2\text{-}400$	2.94
$50 \mathrm{wt}\%\mathrm{C}\text{-TiO}_2\text{-}400$	3.17

250 have the same band gap of 2.80 eV, but the latter one a has higher photocatalytic activity of 50.44% due to the carbon modification that has a better dye adsorption capability. The similar band gap narrowing results are observed in Figure 7(b). The band gaps are reduced from 3.05 eV to 2.66 eV and it is observed that the photocatalytic activities are increased from 49.06% to 84.97%. This is because more excitons could be formed, then heightening the charge separation and transfer process [33]. In Figure 7(c), the band gaps are increased from 3.00 eV to 3.17 eV instead of decreasing after addition of carbon. However, an increase of photocatalytic activity from 48.24% to 70.22% is observed, followed by a decrease of photocatalytic activity from 70.22% to 44.11%. This is because the band gap is large, the electrons need more energy to across over the band gap, thus causing fast electron-hole recombination rate and less active sites for reaction.

3.4 Photoluminescence (PL) Analysis

Figure 8 shows PL spectra of calcination temperature (250, 300, and 400 °C) for (a) 10wt%C-TiO₂, (b) 30wt%C-TiO₂ and (c) 50wt%C-TiO₂. The effects of carbon loadings and calcination temperature in carbon-doped TiO₂ towards charge transfer are discussed. During the calcination process, the carbon is either

decomposed or carbonised with increasing temperature, then the deposited carbon onto TiO₂ would penetrate into TiO2 lattice framework to give Ti-C bond or carbon-doped TiO2. The carbon materials are used as electron traps or scavengers [35] in conjuncture with oxygen vacancies also play the same role in suppressing rapid electronhole recombination. Additionally, vacancies also introduce localized states within the TiO2 band gap, reducing the band gap energy and enabling better absorption of visible light. The sufficient amount of carbon could prevent those oxygen vacancies from neutralized by O2 in the air. The anatase TiO2 shows emission PL peaks at around 500 - 520 nm, which attributed to surface oxygen vacancies (SOVs), meanwhile, no selftrapped exciton (STEs, 420 - 430 nm) and bulk oxygen vacancies (BOVs, 590 - 640 nm) are observed [16].The electron-hole activity contributes significantly to photodegradation efficiency.

Based on Figure 8(a), the lowest PL intensity is 10wt%C-TiO₂-400, while both 10wt%C-TiO₂-250 and 10wt%C-TiO₂-300 display higher intensity. It might be attributed to 10 wt% of carbon was completely burnt off at 400 °C and no carbon left on the TiO₂ surface, causing the SOVs are totally eliminated by O₂ in the air. The loss of SOVs result in the lowest PL intensity for

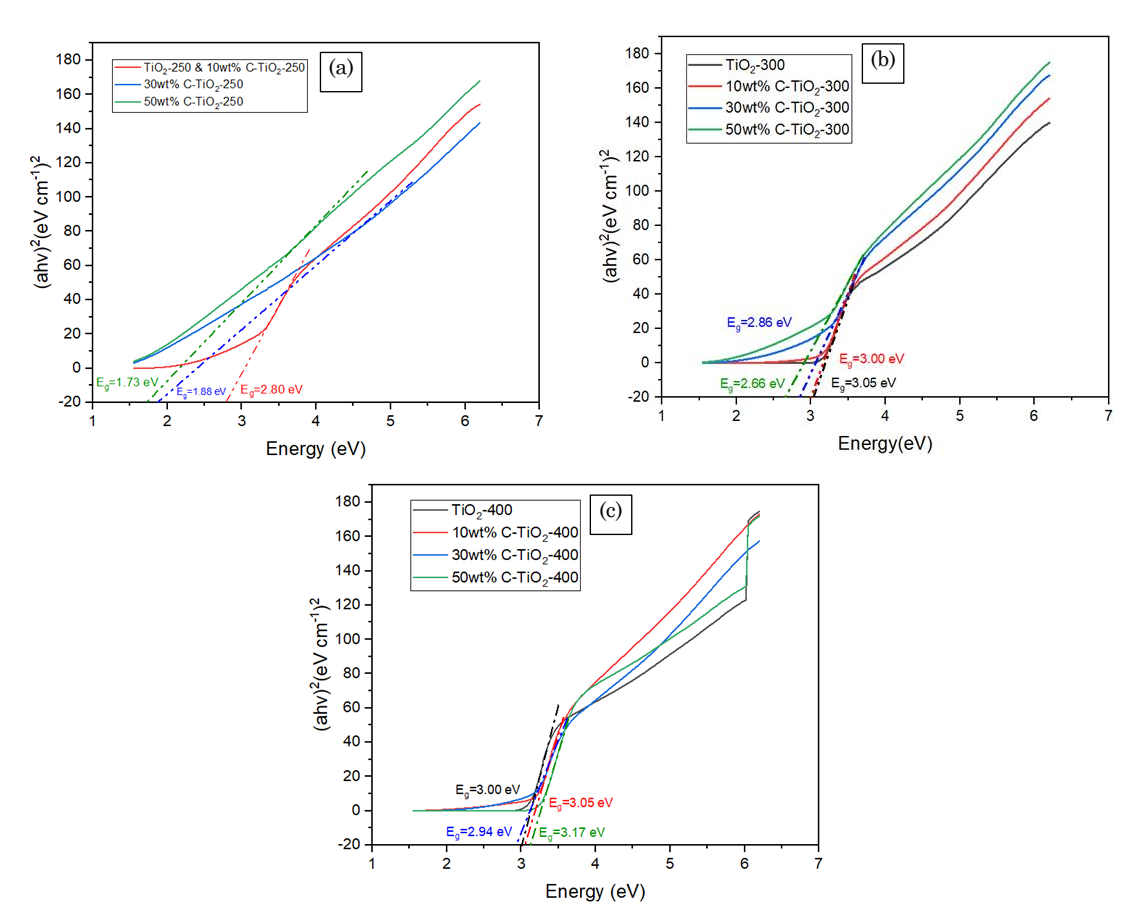


Figure 7. Comparisons of Tauc Plot for carbon-doped TiO_2 with different amount of carbon dopants at calcination temperatures of (a) 250 °C, (b) 300 °C, and (c) 400 °C.

10wt%C-TiO2-400. In Figure 8(b), the amount of carbon loading was increased from 10 to 30 wt%. The 30wt%C- TiO₂-250 exhibited the lowest intensity, while 30wt%C-TiO2-300 and 30 wt%C-TiO₂-400 showed higher intensities, indicating successful carbon incorporation into the TiO₂ lattice and the formation of sufficient SOVs. The presence of moderate SOVs lowers the exciton level, facilitating enhanced charge separation. Similarly, an optimal carbon doping concentration introduces impurity states within the TiO2 band gap, reducing its band gap energy and improving visible-light absorption. As a result, this photocatalyst (30wt%C-TiO₂-250) demonstrated the highest MB photodegradation efficiency. In Figure 8(c), the carbon loading adopted is 50 wt% and 50wt%C-TiO2-250 shows the lowest intensity due to the same reason as 30wt%C-TiO₂-250, thus resulting as the second ranked in the MB photodegradation. The photocatalysts, 30wt%C-TiO2-300, 30wt%C-TiO2-400, 50wt%C-TiO₂-300 and 50wt%C-TiO₂-400, exhibited at higher PL intensities might be due to excess carbon deposited on TiO2 surface, hence, preventing the pollutant adsorption and lowering photodegradation efficiencies. Our findings are in agreement with the past literatures [16,32].

3.5 Photocatalytic Activity and Kinetic Study

3.5.1 Photocatalytic activity

In Figure 9(a), an increasing trend of MB photodegradation of carbon-doped TiO₂ at 250 °C is observed. It indicates that increasing in carbon dopant amounts result in increasing photodegradation from 42.50% to 89.5%, due to narrow band gap, incorporation of carbon into TiO₂ lattice, and sufficient SOVs are formed. Besides that, in Figure 9(b), the photodegradation rate for carbon-doped TiO2 calcined at 300 °C increases from 49.06% to 84.97% when the carbon amount has increased. In Figure 9(c), the photodegradation rate increases from 48.24% to 70.22% for undoped TiO₂-400 and 10wt%C-TiO₂-400. This can be explained by modification in the structure of the TiO2 due to addition of carbon dopants could lead to a higher light absorption range and promote the generation of electron-hole pairs. However, once it has reached a certain point, excess carbon amount will lead to a higher recombination rate of electron-hole pairs and slow down the photocatalytic process, therefore the photodegradation rate decreased to 44.11% for 50wt%C-TiO₂-400.

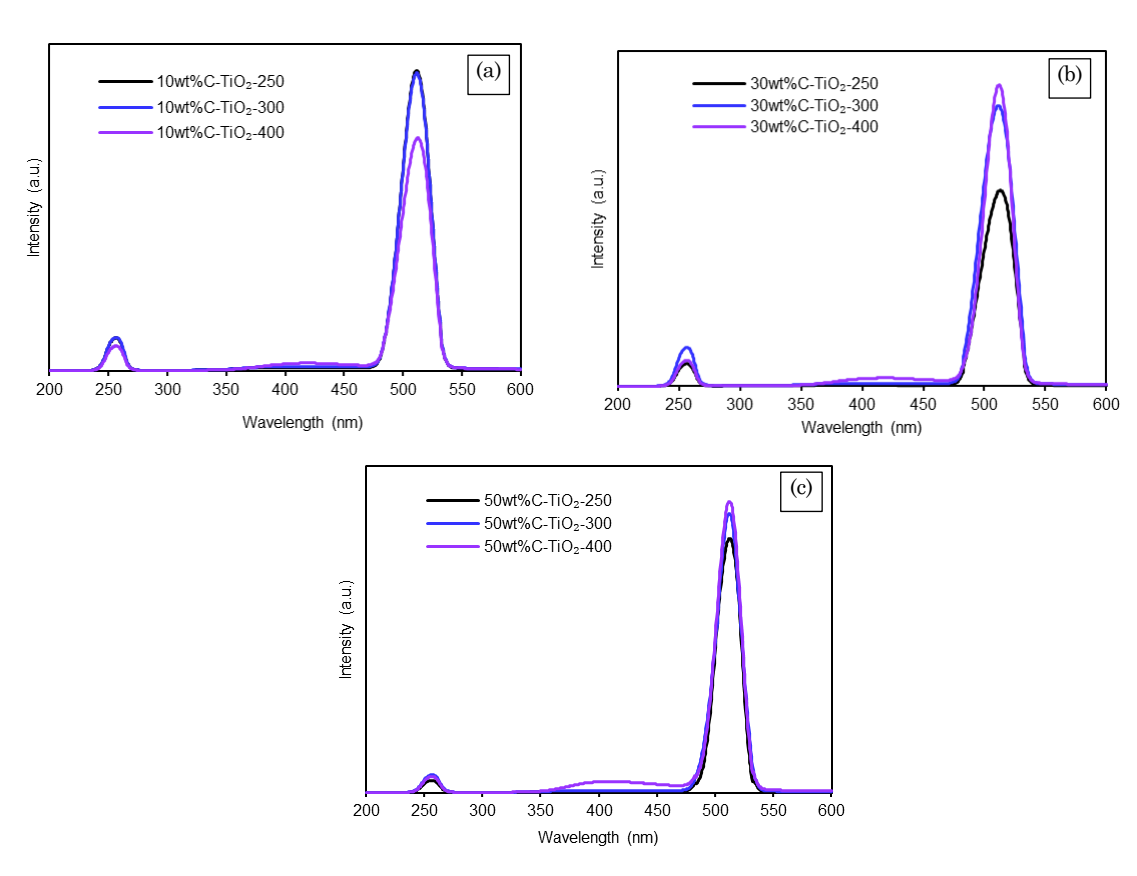


Figure 8. PL spectra of different calcination temperature for (a) 10wt%C-TiO₂, (b) 30wt%C-TiO₂ and (c) 50wt%C-TiO₂.

In Figure 10(a), pristine TiO₂ which calcined at 300 °C has the highest photocatalytic activity with 49.06% due to narrower band gap. In Figure 10(b), the photodegradation conversion of

10wt%C-TiO₂ increases from 50.44% to 70.22% when the calcination temperature increases due to narrow band gap, incorporation of carbon into TiO₂ lattice, and sufficient SOVs are formed. This

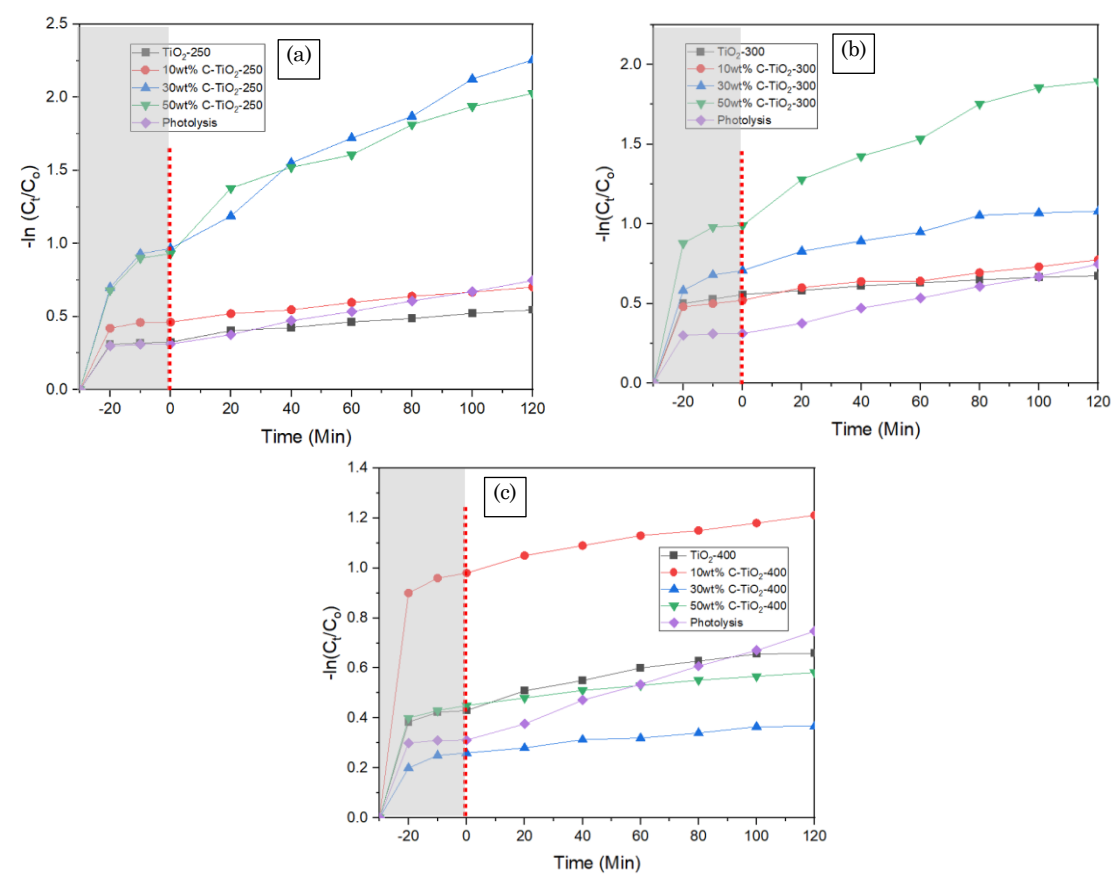


Figure 9. Plot of $-\ln(C_t/C_o)$ versus time (min) for the photodegradation of methylene blue using TiO_2 and carbon-doped TiO_2 samples with different carbon amounts at (a) 250 °C, (b) 300 °C, and (c) 400 °C.

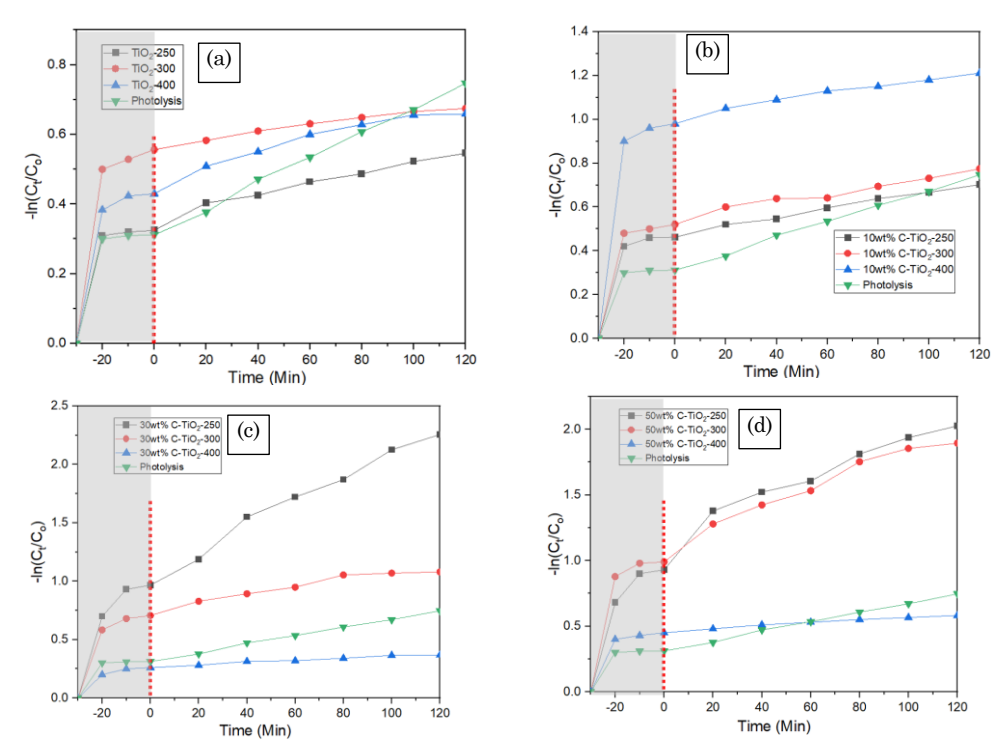


Figure 10. Plot of $-\ln(C_{\text{t}}/C_{\text{o}})$ versus time (min) for the photodegradation of methylene blue using (a) TiO₂ and carbon-doped TiO₂ samples with different calcination temperatures at carbon amounts of (b) 10 wt%, (c) 30 wt%, and (d) 50 wt%.

subsequently enhances the overall photocatalytic process by providing more reactive sites [32]. However, in Figure 10(c), the photodegradation conversion for 30wt%C-TiO2 decreases from 89.53% to 30.74%. In Figure 10(d), the decreasing trend is also noticed, which decreasing from 86.82% to 44.11% for $50\text{wt}\%\text{C-TiO}_2$ when the calcination temperature increases from 250 to 400 °C. This is because excess carbon deposited on TiO₂ surface, hence, lowering photodegradation efficiencies.

Based on Figure 11, the colours of MB are fading, from dark blue to faint blue, indicating the photocatalysts have successfully degraded the MB pollutants. This residual colour is a result of the 2-hour time limit we imposed for our experiments, which focused primarily on calculating the degradation rate rather than determining the total time required for complete degradation. In our findings, the most effective sample, 30wt%C-TiO₂ at 250 °C, achieved a degradation conversion of 89.53% within the 2-hour timeframe. This indicates to a degradation rate of 44.765% per

The adsorption of MB onto the TiO₂ catalyst surface is a crucial prerequisite for effective photodegradation. In acidic conditions, MB carries a positive charge, leading to electrostatic repulsion with Ti4+, which is not favourable for adsorption. Conversely, in alkaline solutions, TiO2 surface becomes negatively charged, allowing the electrostatic attraction and adsorption of the cationic dye, MB. As a result, the colour of the solution fades even in the dark due to strong adsorption rather than MB undergoing direct degradation. Additionally, alkaline conditions provide an environment conducive photocatalysts that are rich in hydroxyl groups. This enhances the formation of oxidative hydroxyl radicals (•OH), which are highly effective in degrading and decomposing organic molecules. Table 5 summarizes the comparisons of photocatalytic degradation of MB using carbondoped TiO2 under various conditions.

3.5.2 Kinetic study

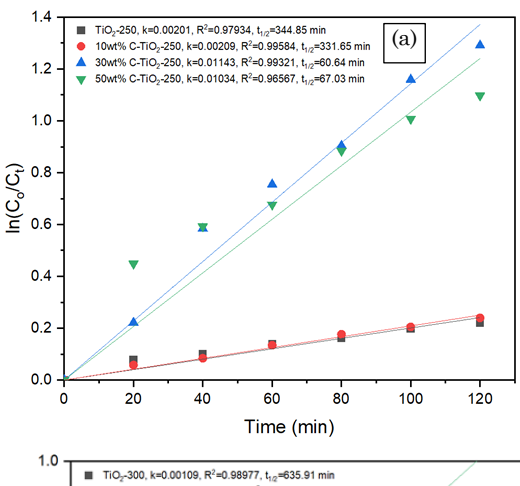
First order Langmuir-Hinshelwood (LH) kinetic model is followed to determine the MB concentration change:

$$\ln C_t = -kt + \ln C_0 \tag{2}$$

$$\ln C_t = -kt + \ln C_0$$

$$\ln \frac{c_0}{c_t} = kt$$
(2)

The experimental data are plotted and linearized in Figure 12, where the slope refers to degradation rate constant influenced concentration. A steeper slope indicates a higher



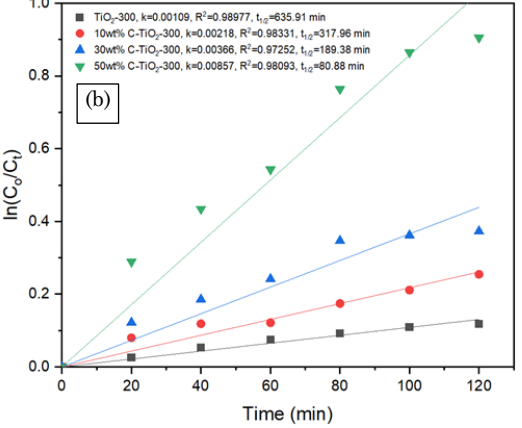




Figure 11. The collection of degraded methylene blue samples every 20-min interval under visiblelight irradiation (300 W) for 2 h.

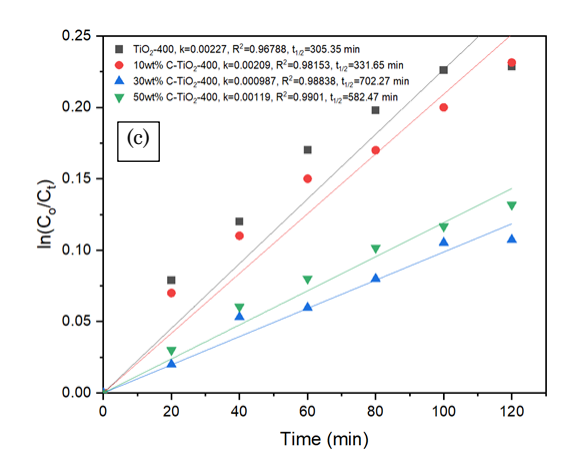


Figure 12. 1st order linear regression of kinetic data on MB photodegradation under visible light irradiation for 2 h with C-TiO₂ samples with different carbon amounts of 10wt%, 30wt% and 50wt% at (a) 250 °C, (b) 300 °C, and (c) 400 °C.

rate constant and better photodegradation efficiency. Half-life time was also determined based on 0.693/k to figure out the time required for MB concentration to decrease to one-half of the initial concentration. The shorter half-life time is favourable as the catalyst performs to be more efficient.

The experimental results fit well with the linearized model with R² falling between 0.96567 to 0.9958 in Figure 12 (a) to (c), thus the data are reliable and significant to analyse the efficiency of C-TiO₂ in MB photodegradation. Figure 12 (a) displays different carbon loading at calcination temperature of 250 °C, and 30wt% C-TiO2 is most efficient as it shows the shortest half-life time of MB degradation which is $t_{1/2}$ = 60.64 min. Additionally, this result is reliable and applicable as the R² reaches 0.99321. Among the three different calcination temperatures, the photocatalyst with carbon doping under 250 °C presents the highest efficiency with shorter halflife time, owing to its remaining bidentate carboxylate ligands (O-Ti-C) to act as the chargetransfer complex at lower temperature; hence, resulting in a better photodegradation performance.

3.6 Reaction Mechanisms

The carbon-doped TiO₂ exhibits better photocatalytic efficiency compared to bare TiO₂, which attributing to 2 possible reasons: (1) the carbons located at the oxygen lattice of TiO₂ to create impurity level that the excited electrons could rapidly jump from the valance band via impurity level to conduction band, thus narrowing the band gap to visible absorption region; (2) the MB dye adsorbs onto carbons. The deposited carbons with COOH group on the TiO2 surface could trap and transfer the excited electrons for better charge separation and electron conductivity, heightening the thus photodegradation efficiency.

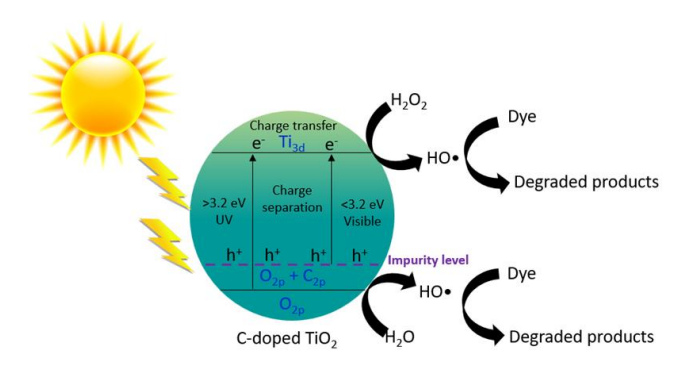


Figure 13. The proposed photodegradation mechanism on carbon-doped TiO_2 with narrower band gap, enhanced charge separation, and reduced charge transfer resistance.

In detail (Figure 13), photocatalysis begins with the electron excitation by absorbing light on CB. Carbon may occupy the cationic sites in the lattice of TiO2 to create an impurity level and the effective light range is prolonged to visible light range. Electrons are irradiated to form e^{-h} pairs and migrate to the surface of catalyst and further generate reactive oxygen species, which are highly active in photodegradation reaction. Oxygen traps photo-generated electrons to form O2- and •OH which may attack and degrade organic molecules by oxidation. Carboxylic group (-COOH) and TiO2 could form bidentate carboxylate ligands O-Ti-C to act as the charge-transfer complex, which is more powerful than solely hydroxyl group. Apart from the formation of principal oxidative hydroxyl radicals (•OH) due to hydroxyl group (-OH), carbonyl group could trap and transfer electrons to facilitate charge separation. The strong electron-withdrawing capability of carboxylic group contributes to increased electron transfer and improved efficiency. Our findings are in alignment with the past literatures [36,37].

4. Conclusions

photocatalyst, carbon doped-TiO₂ (xwt%C-TiO2-y, x=loading amount and y=calcined temperature), with 10, 30, and 50 wt% of ascorbic acid has been successfully synthesized through solvothermal treatment and calcination (250, 300, and 400 °C). The carbon-doped TiO2 has been formed as proven by the diffractogram peaks slightly shifted to lower degree with increasing of carbon loadings. The carbon materials bonded TiO₂ lattice act as electron traps or scavengers, and moderate amount of surface oxygen vacancies through carbon created doping calcination. The 100% anatase TiO2, which is effective in photodegradation has been generated. The reduction of band gaps (1.73 and 1.88 eV) and surface oxygen vacancies have enhanced the electron-hole pair excitation for charge separation and interfacial charge transfer. The presence of C=C and C=O groups could effectively enhance electronic conductivity and attract MB for surface adsorption, further heightening photodegradation. In a nutshell, the carbon doping onto TiO₂ resulted in a better performance on the photodegradation under visible-light irradiation for 2 h. Among the photocatalysts, 30wt%-TiO₂-250 achieved the optimum performance of 89.53% at pH of 10. Nonetheless, future recommendations challenges the or regarding to scalability and full-scale implementation of this research mainly focus on three aspects: (1) Light penetration - high pollutant concentration in wastewater will hinder penetration thus limit photodegradation efficiency. Pre-treatment is essential to reduce the concentration of pollutants

before applying photodegradation to ensure the high efficiency. Some pre-treatment techniques, for instances, flocculation, biological treatment, and ozone-based oxidation can be employed to reduce the pollutant concentration; (2) Reaction condition – the complexity in wastewater involves pH, temperature and the presence of other substances when scaling up the process. Further researches can be conducted to optimize the reaction conditions with regard to the affecting factors; and (3) Economic factor – utilization of visible lights in a large scale could result in high expenses. Research should be driven towards LED lights or solar simulated lights which are more energy-saving and economic.

Acknowledgment

The work is supported by Xiamen University Malaysia Research Fund (grant number: XMUMRF/2019-C4/IENG/0019, XMUMRF/2020-C5/IENG/0029, and XMUMRF/2025-C15/IENG/0077).

CRediT Author Statement

Authors Contributions: Alysa Lau: Investigation, Project administration, Validation, Project administration, Writing - original draft; Chien Yong Goh: Formal analysis, Data curation; Yubei Guo: Writing - original draft; Abdulkareem Ghassan Alsultan: Methodology, Investigation; Yun Hin Taufiq-Yap: Conceptualization, Resources; Mukhamad Nurhadi: Conceptualization; Sin Yuan Lai: Conceptualization, Funding acquisition, Methodology, Supervision, Resources, Visualization, Writing - original draft; Writing review & editing. All authors have read and agreed to the published version of the manuscript.

References

- [1] Hudd, A. (2022). Dyeing for fashion: Why the clothes industry is causing 20% of water pollution.

 URL: https://www.euronews.com/green/2022/02/26/dyeing-for-fashion-why-the-fashion-industry-is-causing-20-of-water-pollution
- [2] Stokes, J. (2023). Textile industry: water management. *URL:* https://pciaw.org/textile-industry-water-management/
- [3] Gómez-Avilés, A., Peñas-Garzón, M., Bedia, J., Rodriguez, J.J., Belver, C. (2019). C-modified TiO2 using lignin as carbon precursor for the solar photocatalytic degradation of acetaminophen. *Chemical Engineering Journal*, 358, 1574–1582. DOI: 10.1016/j.cej.2018.10.154.
- [4] Wu, X., Yin, S., Dong, Q., Guo, C., Li, H., Kimura, T., Sato, T. (2013). Synthesis of high visible light active carbon doped TiO2 photocatalyst by a facile calcination assisted solvothermal method. *Applied Catalysis B: Environmental*, 142–143, 450–457. DOI: 10.1016/j.apcatb.2013.05.052.
- [5] Negi, C., Kandwal, P., Rawat, J., Sharma, M., Sharma, H., Dalapati, G., Dwivedi, C. (2021). Carbon-doped titanium dioxide nanoparticles for visible light driven photocatalytic activity. *Applied Surface Science*, 554 DOI: 10.1016/j.apsusc.2021.149553.
- [6] Mkhalid, I.A., Ismail, A.A., Hussein, M.A., Al thomali, R.H.M. (2023). Visible-light-induced V2O5-TiO2 photocatalysts with high photocatalytic ability for degradation of tetracycline. Optical Materials, 135, 113263. DOI: 10.1016/j.optmat.2022.113263.
- [7] Lee, H., Jang, H.S., Kim, N.Y., Joo, J.B. (2021). Cu-doped TiO2 hollow nanostructures for the enhanced photocatalysis under visible light conditions. *Journal of Industrial and Engineering Chemistry*, 99, 352–363. DOI: 10.1016/j.jiec.2021.04.045.

Table 5. The photocatalytic degradation of MB using carbon-doped TiO₂ under various conditions. (PDADMAC is the abbreviation of polydiallyldimethylammonium chloride).

		Reaction Conditions					Degrada	Rate	No. of		
Carbon sources	Cationic dyes	Catalyst amount (g/L)	Pollutant Concent. (mg/L)	pН	Light power (W)	Reaction time (h)	Degradat ion (%)	tion rate (h-1)	constant (×10 ⁻³ min ⁻¹)	reuse cycles	Ref.
PDADMAC	Methylene blue	0.5	10-5	10	300	2	-	-	45.13	4	[5]
Glucose	Rhodamine B	1.0	10	-	175	1	-	-	48.4		[16]
Poly(ethylene glycol)	Rhodamine B	1.0	10	-	175	1	-	-	66.6	-	[16]
Poly(vinyl alcohol)	Rhodamine B	1.0	10	-	175	1	-	-	7.7	-	[16]
Carbon black	Methylene blue	0.4	30	-	150	2	-	-	32.8	-	[38]
Ethanol	Methylene blue	0.5	25	-	-	2	-	-	12.05	-	[14]
Citric acid/ethylene glycol	Methylene blue	1.0	10	3	-	100 min	60	36	-	-	[20]
Citric acid/ethylene glycol	Methylene blue	1.0	10	7	-	80 min	100	75	-	-	[20]
Citric acid/ethylene glycol	Methylene blue	1.0	10	10	-	40 min	100	150	-	-	[20]
Ascorbic acid	Methylene blue (cationic)	0.2	25	10	300	2	89.53	44.77	11.43	-	Our study

- [8] Kumari, N., Chintakula, S., Sai Sonali Anantha, I., Maddila, S. (2023). An efficient P3TA/Fe doped TiO2 catalyst for photo-degradation of Brilliant green dye and inactivation of pathogens under visible light. Results in Chemistry, 5, 100759. DOI: 10.1016/j.rechem.2022.100759.
- [9] Zhang, Z., Zhao, C., Duan, Y., Wang, C., Zhao, Z., Wang, H., Gao, Y. (2020). Phosphorus-doped TiO2 for visible light-driven oxidative coupling of benzyl amines and photodegradation of phenol. Applied Surface Science, 527, 146693. DOI: 10.1016/j.apsusc.2020.146693.
- [10] Jiang, L., Luo, Z., Li, Y., Wang, W., Li, J., Li, J., Ao, Y., He, J., Sharma, V.K., Wang, J. (2020). Morphology- and Phase-Controlled Synthesis of Visible-Light-Activated S-doped TiO2 with Tunable S4+/S6+ Ratio. Chemical Engineering Journal, 402, 125549. DOI: 10.1016/j.cej.2020.125549.
- [11] Guan, S., Cheng, Y., Hao, L., Yoshida, H., Tarashima, C., Zhan, T., Itoi, T., Qiu, T., Lu, Y. (2023). Oxygen vacancies induced band gap narrowing for efficient visible-light response in carbon-doped TiO2. Scientific Reports, 13(1), 14105. DOI: 10.1038/s41598-023-39523-6.
- Adel Hamza, M., Abd El-Rahman, S.A., [12]Ramadan, S.K., Ezz-Elregal, E.-E.M., Rizk, S.A., Abou-Gamra, Z.M. (2024). The enhanced visiblelight-driven photocatalytic performance nanocrystalline TiO2 decorated by quinazolinone-photosensitizer toward photocatalytic treatment of simulated wastewater. Journal of Photochemistry and Photobiology A: Chemistry, 452, 115599. DOI: 10.1016/j.jphotochem.2024.115599.
- [13] Zhao, J., Wang, B., Zhao, Y., Hou, M., Xin, C., Li, Q., Yu, X. (2023). High-performance visible-light photocatalysis induced by dye-sensitized Ti3+-TiO2 microspheres. *Journal of Physics and Chemistry of Solids*, 179, 111374. DOI: 10.1016/j.jpcs.2023.111374.
- [14] Matos, J., García, A., Zhao, L., Titirici, M.M. (2010). Solvothermal carbon-doped TiO2 photocatalyst for the enhanced methylene blue degradation under visible light. Applied Catalysis A: General, 390(1–2), 175–182. DOI: 10.1016/j.apcata.2010.10.009.
- [15] Zhong, J., Chen, F., Zhang, J. (2010). Carbon-deposited TiO2: Synthesis, characterization, and visible photocatalytic performance. *Journal of Physical Chemistry C*, 114(2), 933–939. DOI: 10.1021/jp909835m.
- [16] Teng, F., Zhang, G., Wang, Y., Gao, C., Chen, L., Zhang, P., Zhang, Z., Xie, E. (2014). The role of carbon in the photocatalytic reaction of carbon/TiO2 photocatalysts. *Applied Surface Science*, 320, 703–709. DOI: 10.1016/j.apsusc.2014.09.153.
- [17] Kavitha, R., Devi, L.G. (2014). Synergistic effect between carbon dopant in titania lattice and surface carbonaceous species for enhancing the visible light photocatalysis. *Journal of Environmental Chemical Engineering*, 2(2), 857–867. DOI: 10.1016/j.jece.2014.02.016.

- [18] Park, Y., Kim, W., Park, H., Tachikawa, T., Majima, T., Choi, W. (2009). Carbon-doped TiO2 photocatalyst synthesized without using an external carbon precursor and the visible light activity. *Applied Catalysis B: Environmental*, 91(1–2), 355–361. DOI: 10.1016/j.apcatb.2009.06.001.
- [19] Ghime, D., Mohapatra, T., Verma, A., Banjare, V., Ghosh, P. (2020). Photodegradation of aqueous eosin yellow dye by carbon-doped TiO2 photocatalyst. In: *IOP Conference Series: Earth* and Environmental Science. IOP Publishing LtdDOI: 10.1088/1755-1315/597/1/012010.
- [20] Xiao, Q., Zhang, J., Xiao, C., Si, Z., Tan, X. (2008). Solar photocatalytic degradation of methylene blue in carbon-doped TiO2 nanoparticles suspension. Solar Energy, 82(8), 706–713. DOI: 10.1016/j.solener.2008.02.006.
- [21] Carbajo, J., Adán, C., Rey, A., Martínez-Arias, A., Bahamonde, A. (2011). Optimization of H2O2 use during the photocatalytic degradation of ethidium bromide with TiO2 and iron-doped TiO2 catalysts. *Applied Catalysis B: Environmental*, 102(1–2), 85–93. DOI: 10.1016/j.apcatb.2010.11.028.
- [22] Rasoulnezhad, H., Kavel, G.K., Ahmadi, K., Rahimipour, M.R. (2017). Combined sonochemical/CVD method for preparation of nanostructured carbon-doped TiO2 thin film. *Applied Surface Science*, 408, 1–10.
- [23] Qi, D., Xing, M., Zhang, J. (2014). Hydrophobic carbon-doped TiO2/MCF-F composite as a high performance photocatalyst. *Journal of Physical Chemistry C*, 118(14), 7329–7336. DOI: 10.1021/jp4123979.
- [24] Astuti, Y., Musthafa, F., Arnelli, A., Nurhasanah, I. (2022). French Fries-Like Bismuth Oxide: Physicochemical Properties, Electrical Conductivity and Photocatalytic Activity. Bulletin of Chemical Reaction Engineering and Catalysis, 17(1), 146–156. DOI: 10.9767/BCREC.17.1.12554.146-156.
- [25] Sunardi, A.B.T., Choirunnisa, F., Dewi, A.S.P., Widiyandari, H., Astuti, Y., Arutanti, O., Salim, A.A., Mufti, N. (2025). Enriched photocatalytic degradation of methylene orange dye using carbon quantum dots surface-decorated TiO2 nanocomposites. *Materials Chemistry and Physics*, 329 DOI: 10.1016/j.matchemphys.2024.130049.
- Al-Amin, M., Dey, S.C., Rashid, [26] T.U., Ashaduzzaman, M., Shamsuddin, S.M. (2016). Solar Assisted Photocatalytic Degradation of Reactive Azo Dyes in Presence of Anatase Titanium Dioxide Alkylation of cresols View Solar Assisted Photocatalytic Degradation of Reactive Azo Dyes in Presence of Anatase Titanium Dioxide. International Journal of Latest Research in Engineering and Technology (IJLRET,2, 14-21.10.1016/j.solmat.2003.11.022

- [27] Li, W., Liang, R., Zhou, N.Y., Pan, Z. (2020). Carbon Black-Doped Anatase TiO2 Nanorods for Solar Light-Induced Photocatalytic Degradation of Methylene Blue. ACS Omega, 5(17), 10042– 10051. DOI: 10.1021/acsomega.0c00504.
- [28] Zhong, J., Chen, F., Zhang, J. (2010). Carbon-deposited TiO2: Synthesis, characterization, and visible photocatalytic performance. *Journal of Physical Chemistry C*, 114(2), 933–939. DOI: 10.1021/jp909835m.
- [29] Jafari, S., Tryba, B., Kusiak-Nejman, E., Kapica-Kozar, J., Morawski, A.W., Sillanpää, M. (2016). The role of adsorption in the photocatalytic decomposition of Orange II on carbon-modified TiO2. Journal of Molecular Liquids, 220, 504–512. DOI: 10.1016/j.molliq.2016.02.014.
- [30] Mert, E.H., Yalçın, Y., Kılıç, M., San, N., Çınar, Z. (2008). Surface Modification of TiO2 with Ascorbic Acid for Heterogeneous Photocatalysis: Theory and Experiment. Journal of Advanced Oxidation Technologies, 11(2) DOI: 10.1515/jaots-2008-0203.
- [31] Simonetti, E.A.N., De Simone Cividanes, L., Campos, T.M.B., De Menezes, B.R.C., Brito, F.S., Thim, G.P. (2016). Carbon and TiO2 synergistic effect on methylene blue adsorption. *Materials Chemistry and Physics*, 177, 330–338. DOI: 10.1016/j.matchemphys.2016.04.035.
- [32] Sean, N.A., Leaw, W.L., Nur, H. (2019). Effect of calcination temperature on the photocatalytic activity of carbon-doped titanium dioxide revealed by photoluminescence study. *Journal of the Chinese Chemical Society*, 66(10), 1277–1283. DOI: 10.1002/jccs.201800389.
- [33] Lin, Y.T., Weng, C.H., Lin, Y.H., Shiesh, C.C., Chen, F.Y. (2013). Effect of C content and calcination temperature on the photocatalytic activity of C-doped TiO2 catalyst. Separation and Purification Technology, 116, 114–123. DOI: 10.1016/j.seppur.2013.05.018.

- [34] Saiful Amran, S.N.B., Wongso, V., Abdul Halim, N.S., Husni, M.K., Sambudi, N.S., Wirzal, M.D.H. (2019). Immobilized carbon-doped TiO2 in polyamide fibers for the degradation of methylene blue. *Journal of Asian Ceramic Societies*, 7(3), 321–330. DOI: 10.1080/21870764.2019.1636929.
- [35] Muniandy, L., Adam, F., Mohamed, A.R., Ng, E.-P., Rahman, N.R.A. (2016). Carbon modified anatase TiO2 for the rapid photo degradation of methylene blue: A comparative study. Surfaces and Interfaces, 5, 19–29. DOI: 10.1016/j.surfin.2016.08.006.
- [36] Ma, Y., Han, L., Ma, H., Wang, J., Liu, J., Cheng, L., Yang, J., Zhang, Q. (2017). Improving the visible-light photocatalytic activity of interstitial carbon-doped TiO2 with electron-withdrawing bidentate carboxylate ligands. *Catalysis Communications*, 95, 1–5. DOI: 10.1016/j.catcom.2017.02.025.
- [37] Basavarajappa, P.S., Patil, S.B., Ganganagappa, N., Reddy, K.R., Raghu, A. V., Reddy, C.V. (2020). Recent progress in metal-doped TiO2, non-metal doped/codoped TiO2 and TiO2 nanostructured hybrids for enhanced photocatalysis. *International Journal of Hydrogen Energy*, 45(13), 7764–7778. DOI: 10.1016/j.ijhydene.2019.07.241.
- [38] Li, W., Liang, R., Zhou, N.Y., Pan, Z. (2020). Carbon Black-Doped Anatase TiO2 Nanorods for Solar Light-Induced Photocatalytic Degradation of Methylene Blue. ACS Omega, 5(17), 10042– 10051. DOI: 10.1021/acsomega.0c00504.